Supplemental Figures

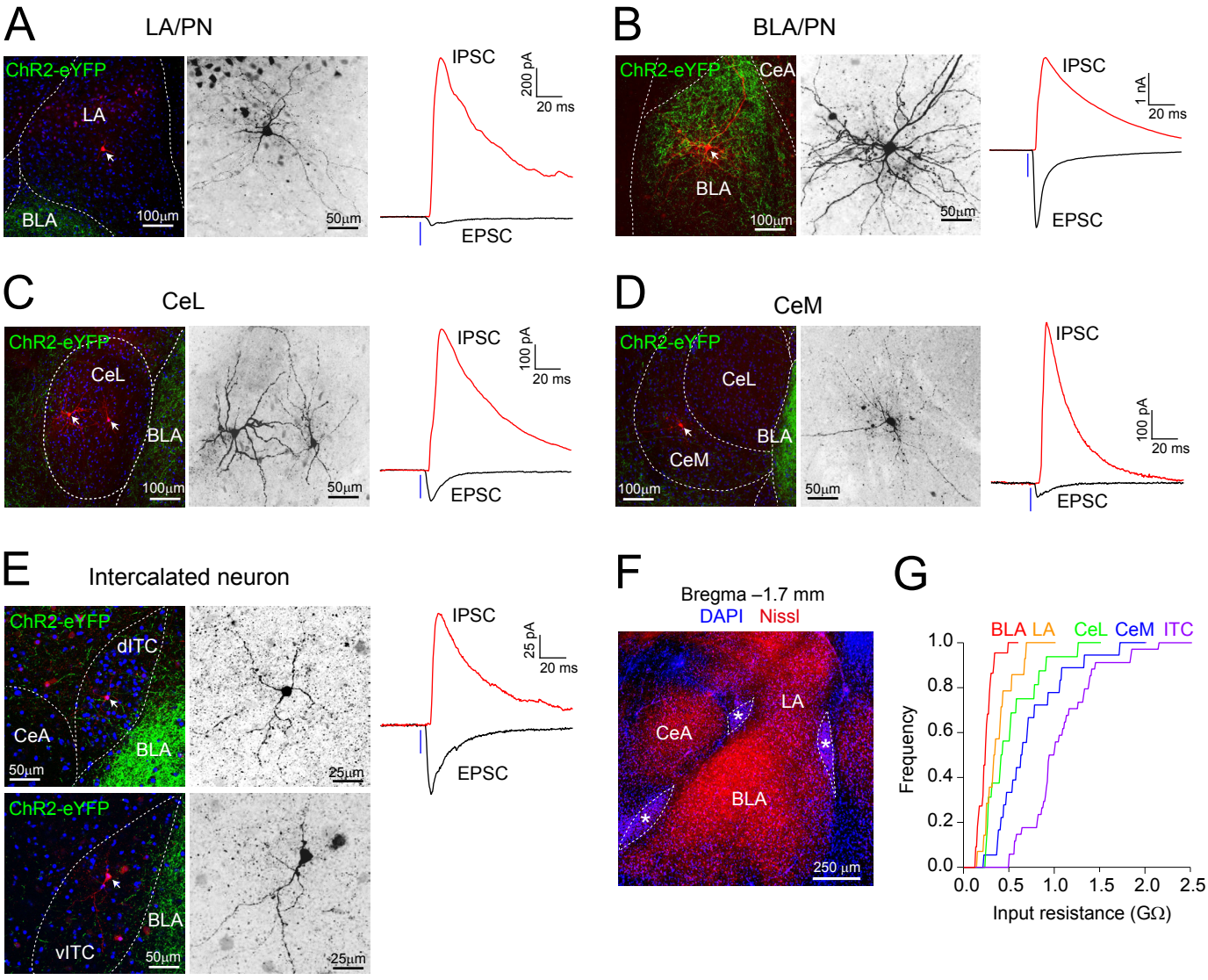

Figure S1

Figure S1, related to Figure 1. Excitatory and Inhibitory Synaptic Responses in Neurons of Different Amygdalar Nuclei Evoked by Photostimulation of mPFC Fibers

(A-E) Left, microscopic images showing the morphology of principal neurons in the lateral nucleus (LA, A) and the anterior division of the basolateral nucleus of the amygdala (BLA, B), neurons in the lateral (CeL, C) and medial divisions (CeM, D) of the central nucleus of the amygdala, and intercalated neurons in dorsal and ventral intercalated cell clusters (dITC and vITC, E). Neurons were loaded with the pipette solution containing 5 mM biocytin, and visualized with streptavidin, Alexa 568 conjugate (red fluorescence, white arrows). Projections arising from ChR2-eYFP expressing neurons in the mPFC are seen as green fluorescence. Right (in each panel from A to E), traces of EPSCs (black) and IPSCs (red) recorded in neurons in each of the above-mentioned nuclei. EPSCs and IPSC were recorded in voltage-clamp mode at –80 mV or 0 mV, respectively. Synaptic responses in different cells were induced by photostimuli of the same intensity (12.5 mW/mm^2, 1-3 ms duration, blue vertical lines) delivered to ChR2-expressing mPFC fibers.
(F) Fluorescent image of the amygdala showing clusters of intercalated neurons (asterisks). Small cytoplasm-to-nucleus ratio makes clusters of intercalated neurons readily distinguishable from other nuclei of the amygdala in merged fluorescent images of DAPI (blue fluorescent, nuclear stain) and Nissl stain (red fluorescence, cytoplasmic stain). Dotted lines indicate margins of clusters of intercalated neurons.
(G) Cumulative histogram showing the distribution of input resistance values for neurons in different nuclei of the amygdala. Note large input resistance of intercalated (ITC) neurons compared to other neurons in the amygdala. n = 22, 14, 16, 18, and 34 cells for neurons in the BLA, LA, CeL, CeM, and intercalated neurons, respectively.
(H) Summary graph showing rates at which excitatory and inhibitory responses could be observed in the course of recordings in different nuclei. Response rates were calculated by dividing the number of neurons displaying EPSC or IPSC (light stimulus intensity was 12.5 mW/mm^2, 1-3 ms duration) by the total number of neurons examined (EPSC: n = 13, 215, 146, 19, and 33 neurons for LA, BLA, ITC, CeL, and CeM, respectively; IPSC: n = 8, 70, 9, 15, and 31 neurons for LA, BLA, ITC, CeL, and CeM, respectively). Note that polysynaptic IPSCs were observed in most neurons regardless of nuclei whereas EPSCs were detected more commonly in BLA principal neurons and ITC neurons compared to LA, CeL, and CeM neurons.
(I) Summary plot of average EPSC and IPSC amplitudes in neurons in different nuclei of the amygdala. EPSCs and IPSCs were induced by photostimulation of mPFC fibers (12.5 mW/mm^2, 1-3 ms duration). Note robust EPSC and IPSC responses in BLA principal neurons compared to neurons in other nuclei.
(J) Summary plot showing EPSC/IPSC amplitude ratios in different nuclei of the amygdala. Note larger EPSC/IPSC ratio in BLA principal neurons and ITC neurons compared to LA, CeL, and CeM neurons. Error bars are SEM.

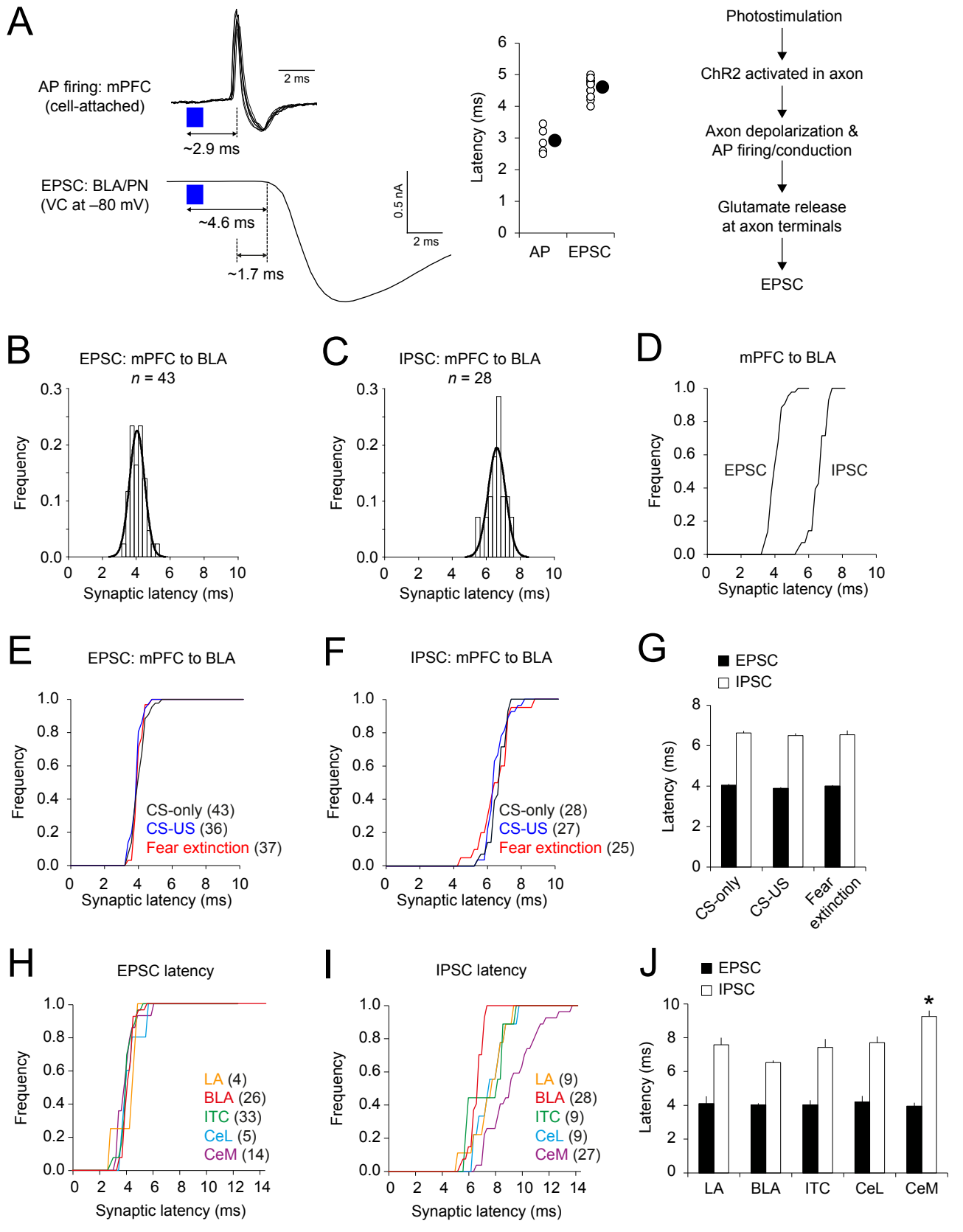
A
AP firing: mPFC
(cell-attached)
2 ms
~2.9 ms
EPSC: BLA/PN
(VC at –80 mV)
~4.6 ms
~1.7 ms
0.5 nA
2 ms
Latency (ms)
AP
EPSC
Photostimulation
ChR2 activated in axon
Axon depolarization &
AP firing/conduction
Glutamate release
at axon terminals
EPSC
B
EPSC: mPFC to BLA
n = 43
Frequency
Synaptic latency (ms)
C
IPSC: mPFC to BLA
n = 28
Frequency
Synaptic latency (ms)
D
mPFC to BLA
EPSC
IPSC
Frequency
Synaptic latency (ms)
E
EPSC: mPFC to BLA
CS-only (43)
CS-US (36)
Fear extinction (37)
Frequency
Synaptic latency (ms)
F
IPSC: mPFC to BLA
CS-only (28)
CS-US (27)
Fear extinction (25)
Frequency
Synaptic latency (ms)
G
EPSC
IPSC
Latency (ms)
CS-only
CS-US
Fear extinction
H
EPSC latency
LA (4)
BLA (26)
ITC (33)
CeL (5)
CeM (14)
Frequency
Synaptic latency (ms)
I
IPSC latency
LA (9)
BLA (28)
ITC (9)
CeL (9)
CeM (27)
Frequency
Synaptic latency (ms)
J
EPSC
IPSC
*
Latency (ms)
LA
BLA
ITC
CeL
CeM

Figure S2

Figure S2, related to Figure 1. Synaptic Latency Analysis in Optogenetically-Evoked EPSCs and IPSCs in the mPFC-Amygdala Pathway

(A) Left, the traces on top are action potentials (AP) recorded in ChR2-expressing pyramidal neurons in the mPFC in a cell-attached recording configuration (multiple APs are superimposed). Average delay from the onset of photostimulation (4.1 mW/mm^2, 1 ms duration, blue square) to the AP peak was 2.9 ms. A lower trace shows the EPSC recorded in a BLA principal neuron (BLA/PN) at –80 mV in voltage clamp-mode. The EPSC was induced by photostimulation of projections from the mPFC (4.1 mW/mm^2, 1 ms duration, blue square). Average delay from the onset of photostimulation to the onset of the EPSC was 4.6 ms. Based on these measurements, synaptic latency was estimated to be ~1.7 ms. Middle, summary graph showing delays from the onset of photostimulation to AP firing (n = 5 neurons in the mPFC, left) and to the EPSC onset (n = 16 neurons in the BLA, right). Open circles represent individual experiments, whereas closed circles show average values. Right, the sequence of events from photostimulation of mPFC projections to generation of EPSCs in the BLA/PN.
(B and C) Histograms showing the distribution of synaptic latencies of EPSCs (B) and IPSCs (C) recorded in BLA/PN and evoked by photostimulation of projections from the mPFC (8.2 mW/mm^2, 1 ms duration). Synaptic latency was calculated as a delay from the start of photostimulation to the onset of EPSC or IPSC. Fitted Gaussian curves are overlaid on the histograms.
(D) Cumulative frequency histograms of EPSC and IPSC latencies for data shown in B and C.
(E-F) Cumulative histograms of latencies of EPSCs (E) and IPSCs (F) recorded in BLA/PN in different groups of behaviorally-trained mice. EPSC and IPSC were evoked by photostimulation of projections from the mPFC (8.2 mW/mm^2, 1 ms duration). Numbers in parentheses indicate number of BLA/PN examined in each group.
(G) Summary plot showing average EPSC and IPSC latencies in different groups.
(H-I) Cumulative histograms of latencies of EPSCs (H) and IPSCs (I) recorded in neurons in different nuclei of the amygdala. Numbers in parentheses indicate number of neurons examined.
(J) A summary plot showing average EPSC and IPSC latencies in neurons in different nuclei of the amygdala. IPSC latency was significantly longer in CeM neurons compared to neurons in other nuclei (*$p < 0.05$). Error bars are SEM.

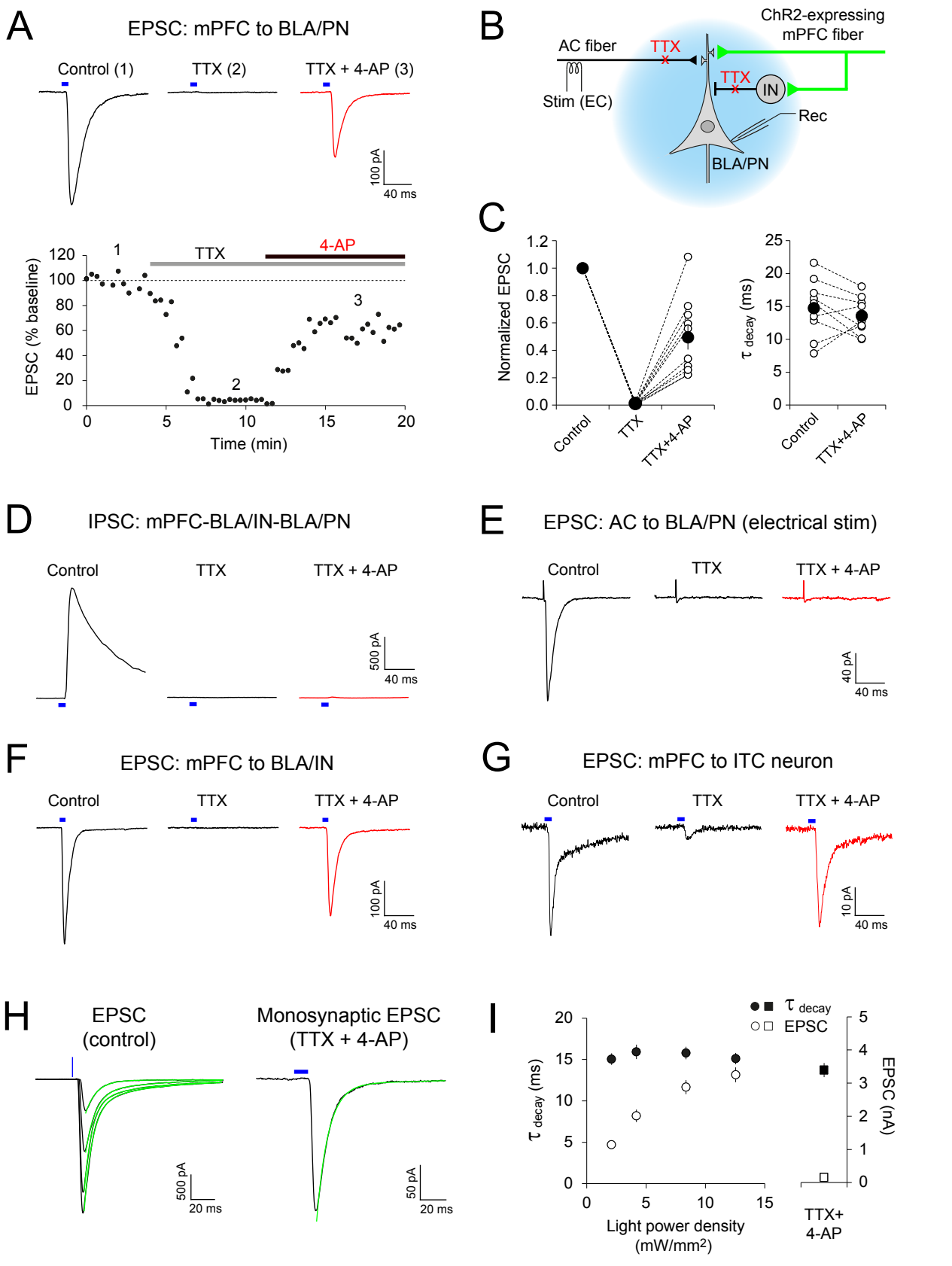
A
EPSC: mPFC to BLA/PN
Control (1)
TTX (2)
TTX + 4-AP (3)
100 pA
40 ms
EPSC (% baseline)
TTX
4-AP
1
2
3
Time (min)
B
ChR2-expressing mPFC fiber
AC fiber
TTX
Stim (EC)
TTX
IN
Rec
BLA/PN
C
Normalized EPSC
Control
TTX
TTX+4-AP
τ decay (ms)
Control
TTX+4-AP
D
IPSC: mPFC-BLA/IN-BLA/PN
Control
TTX
TTX + 4-AP
500 pA
40 ms
E
EPSC: AC to BLA/PN (electrical stim)
Control
TTX
TTX + 4-AP
40 pA
40 ms
F
EPSC: mPFC to BLA/IN
Control
TTX
TTX + 4-AP
100 pA
40 ms
G
EPSC: mPFC to ITC neuron
Control
TTX
TTX + 4-AP
10 pA
40 ms
H
EPSC (control)
Monosynaptic EPSC (TTX + 4-AP)
500 pA
20 ms
50 pA
20 ms
I
τ decay
EPSC
τ decay (ms)
EPSC (nA)
Light power density (mW/mm²)
TTX+ 4-AP

Figure S3

Figure S3, related to Figure 1. Monosynaptic Nature of EPSCs in the mPFC-Amygdala Pathway

(A) Rescue of optogenetically-induced and tetrodotoxin (TTX)-blocked EPSCs by 4-aminopyridine (4-AP). Top, representative EPSCs recorded under different experimental conditions. EPSCs were evoked by photostimulation of ChR2-expressing axons from the mPFC (blue lines), and recorded in a principal neuron in the BLA (BLA/PN) at –80 mV in voltage-clamp mode (1). TTX (1 μM) completely blocked EPSCs (2). Subsequent application of 4-AP (1 mM) in the presence of TTX partially rescued EPSC (3, red trace), indicating monosynaptic nature of connections in the mPFC to the BLA pathway. Longer photostimuli (10 ms) were used to induce EPSCs in the experiments illustrated in this figure. Bottom, a graph showing the time course of the EPSC amplitude changes in the recorded BLA/PN under different conditions. Peak amplitudes of EPSCs were normalized to baseline EPSCs recorded under control conditions. Gray and black horizontal lines within the graph indicate timing of application of TTX and 4-AP, respectively.
(B) Experimental design. Application of 4-AP could rescue TTX-blocked EPSCs only when ChR2-expressing neurons in the mPFC project monosynaptically onto BLA/PN. 4-AP does not rescue TTX-blocked disynaptic IPSC, requiring AP firing in GABAergic interneurons (IN), as interneurons do not express ChR2. 4-AP does not rescue monosynaptic EPSCs, induced by electrical stimulation of the external capsules (EC) containing inputs from the auditory cortex (AC fiber). See Supplemental Text for details.
(C) Summary plots of the EPSC amplitudes (left) and decay time constants (right) in TTX only and TTX + 4-AP. Peak amplitudes of EPSCs were normalized to the baseline EPSC recorded under control conditions. To quantify decay kinetics, decay phase of EPSCs was fitted to the double exponential function, $I(t) = I_f \exp(-t/\tau_f) + I_s \exp(-t/\tau_s)$, where I_f/τ_f and I_s/τ_s are fast and slow components of peak amplitudes and decay time constants of EPSC. Then, weighted mean decay time constant (τ_{decay}) was calculated, $\tau_{decay} = \tau_f[I_f/(I_f + I_s)] + \tau_s[I_s/(I_f + I_s)]$. Note no significant difference in τ_{decay} between control EPSCs and EPSCs in the presence of TTX + 4-AP ($p = 0.29$), suggesting that EPSCs recorded under control conditions reflect monosynaptic EPSCs. Open circles represent individual experiments whereas closed circles show average values (n = 10 neurons from 6 mice).
(D) Representative traces of disynaptic IPSCs (mPFC-BLA/IN-BLA/PN) evoked by photostimulation of projections from the mPFC (blue lines), and recorded in a BLA/PN. The application of 4-AP did not rescue TTX-blocked disynaptic IPSC (red trace). n = 6 neurons from 4 mice.
(E) Representative EPSCs evoked by electrical stimulation of the external capsule-containing projections from the auditory cortex, and recorded in a BLA/PN. The application of 4-AP failed to rescue TTX-blocked EPSC under these conditions (red trace).
(F) Representative traces of EPSCs in the mPFC-BLA/IN pathway in same experiments as in (A-E). EPSCs were evoked by photostimulation of mPFC projections (blue bars), and recorded in interneurons in the BLA (BLA/IN) at –85 mV in voltage-clamp mode (left). EPSCs were blocked by 1 μM TTX (middle). The application of 1 mM 4-AP rescued EPSCs partially in the presence of TTX (right, red trace), suggesting that the

activated connections between mPFC fibers in BLA interneurons were monosynaptic. K^+-based pipette solution was used in these experiments to verify the cell-type of recorded neurons (see Supplemental Experimental Procedures for details). n = 4 interneurons from 3 mice.

(G) Traces of EPSCs evoked by photostimulation of projections from the mPFC (blue lines), and recorded in an intercalated (ITC) neuron. The application of 4-AP rescued TTX-blocked EPSC (red trace) indicating monosynaptic nature of connectivity in the mPFC-ITC pathway.

(H) Left, EPSCs evoked by photostimulation of projections from the mPFC with different light intensities (2.1, 4.2, 8.4, and 12.5 mW/mm^2, 1 ms duration), and recorded in a BLA/PN under control conditions. Right, a monosynaptic EPSC evoked by photostimulation (0.8 mW/mm^2, 10 ms duration), and recorded in a BLA/PN in the presence of TTX (1 μM) and 4-AP (1 mM) as in A. Decay phase of EPSCs was fitted to the double-exponential functions (as in C), which are shown as green curves superimposed onto each EPSC trace.

(I) Left, summary plot showing average decay time constants (τ_{decay}, filled circles) and average peak amplitudes of EPSCs (open circles) recorded in BLA neurons at different light intensities under control conditions as in H (n = 22 neurons from 4 mice). Right, average decay time constant and amplitude of monosynaptic EPSCs recorded in the presence of TTX and 4-AP (square symbols, n = 10 neurons from 6 mice). Decay time constant of EPSC (τ_{decay}) was calculated as in C. Peak amplitudes of EPSCs in the mPFC-BLA pathway were proportional to the light intensity ($p < 0.001$), whereas decay time (τ_{decay}) remained constant over the range of light intensities ($p = 0.78$). Although peak amplitudes were much larger for EPSCs recorded under control conditions than for EPSCs recorded in the presence of TTX and 4-AP, there was no significant difference in decay time constant between these two conditions ($p > 0.78$). Error bars are SEM.

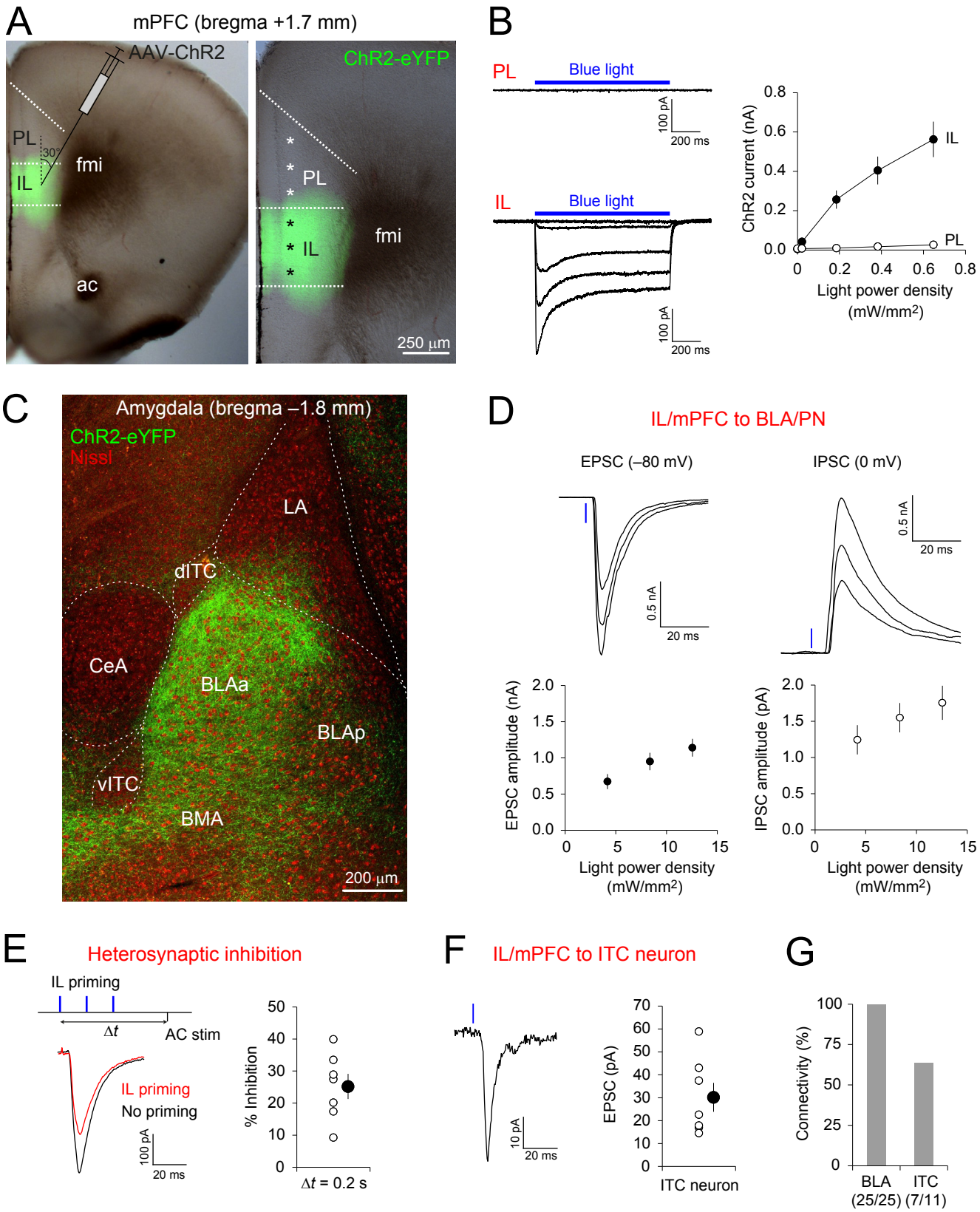
A
mPFC (bregma +1.7 mm)
AAV-ChR2
ChR2-eYFP
PL
30°
fmi
IL
ac
250 μm
B
PL
Blue light
100 pA
200 ms
IL
Blue light
ChR2 current (nA)
Light power density (mW/mm²)
C
Amygdala (bregma –1.8 mm)
ChR2-eYFP
Nissl
LA
dlTC
CeA
BLAa
BLAp
vlTC
BMA
200 μm
D
IL/mPFC to BLA/PN
EPSC (–80 mV)
IPSC (0 mV)
0.5 nA
20 ms
EPSC amplitude (nA)
IPSC amplitude (pA)
Light power density (mW/mm²)
E
Heterosynaptic inhibition
IL priming
Δt
AC stim
IL priming
No priming
100 pA
20 ms
% Inhibition
Δt = 0.2 s
F
IL/mPFC to ITC neuron
10 pA
20 ms
EPSC (pA)
ITC neuron
G
Connectivity (%)
BLA (25/25)
ITC (7/11)

Figure S4

Figure S4, related to Figure 1. Anatomical and Electrophysiological Characterization of Projections Arising from the IL/mPFC in the Amygdala

(A) Microscopic images showing ChR2-eYFP expression (green) localized to the infralimbic division (IL) of the mPFC. Asterisks indicate approximate locations of six neurons we recorded from to examine ChR2-mediated photocurrents (as in B) in the IL and prelimbic division of the mPFC (PL) in each mouse tested. Dotted lines indicate approximate borders between divisions of the mPFC based on the mouse brain atlas by Franklin and Paxinos (2008). fmi: forceps minor of the corpus callosum; ac: anterior commissure.
(B) Left, representative traces of ChR2-mediated photocurrents recorded in PL or IL neurons. Superimposed photocurrents were evoked by different light intensities (0, 0.02, 0.19, 0.38, and 0.65 mW/mm^2). In the IL neuron, 1-s photostimulation pulses induced typical ChR2-mediated currents (lower traces), whereas photostimualtion with the same intensities and duration failed to induce photocurrents in the PL neuron (upper traces). Right, summary graph showing average peak amplitudes of photocurrents in PL and IL neurons. In each mouse, we tested photocurrents in 3-4 IL neurons and 3 PL neurons (in total: 17 IL neurons and 15 PL neurons from 5 mice).
(C) A microscopic image showing projections arising from the IL/mPFC in the amygdala. Note dense projections (green) in the anterior division of the BLA (BLAa). Red fluorescence is Nissl stain. Dotted lines indicate borders between different nuclei of the amygdala. LA, lateral nucleus of the amygdala; BLAa and BLAp, anterior and posterior divisions of the basolateral nucleus of the amygdala; BMA, the basomedial nucleus of the amygdala; dITC and vITC, dorsal and ventral clusters of intercalated neurons, CeA, central nucleus of the amygdala.
(D) Synaptic responses induced by photostimulation of projections from the IL/mPFC and recorded in principal neurons of the BLAa (BLA/PN). Left, traces of EPSCs which were evoked by photostimuli of different intensities (4.2, 8.4, 12.5 mW/mm^2). Right, traces represent IPSCs recorded in the same neuron and evoked by photostimuli of the same intensities as for EPSCs. Input-output curves for EPSCs (filled circles) and IPSCs (open circles) are shown below the EPSC or IPSC traces (n = 20 neurons from 5 mice).
(E) Left, heterosynaptic inhibition of EPSCs in the auditory cortex (AC)-to-BLA pathway by priming activation of projections from the IL/mPFC. Short pulses of light (3 pulses with 50 ms intervals, 1 ms duration) were applied to activate projections from the IL (IL priming, blue lines). After priming stimulation of IL projections (Δt = 0.2 s), the external capsule, containing auditory cortical inputs, was stimulated electrically (AC stim). IL priming decreased the EPSC amplitude in the AC-to-BLA pathway (red trace) compared to no-priming control (black trace). Right, summary graph showing the magnitude of heterosynaptic inhibition as the percentage of inhibition relative to the control EPSC (recorded without priming). Open circles represent individual experiments, and a filled circle indicates averaged heterosynaptic inhibition (n = 7 neurons from 4 mice).
(F) Left, a representative EPSC recorded in an intercalated (ITC) neuron and evoked by photostimulation of projections from the IL/mPFC (left panel). Right, summary plot showing peak EPSC amplitudes in the IL-to-ITC pathway. Photostimulation (12.5 mW/mm^2) induced EPSCs in 7 out of 11 intercalated neurons examined (data are from

4 mice). Open circles correspond to individual experiments; a filled circle shows averaged EPSC amplitude.
(G) A graph illustrating connectivity levels of projections from the IL/mPFC to BLA/PN and to intercalated neurons. Connectivity was calculated as the proportion of neurons displaying EPSCs evoked by photostimulation of IL/mPFC projections to the total number of neurons examined. Numbers in the parentheses indicate the number of neurons displaying EPSCs (left) and the total number of neurons tested (right). Results are from 5 mice. Error bars are SEM.

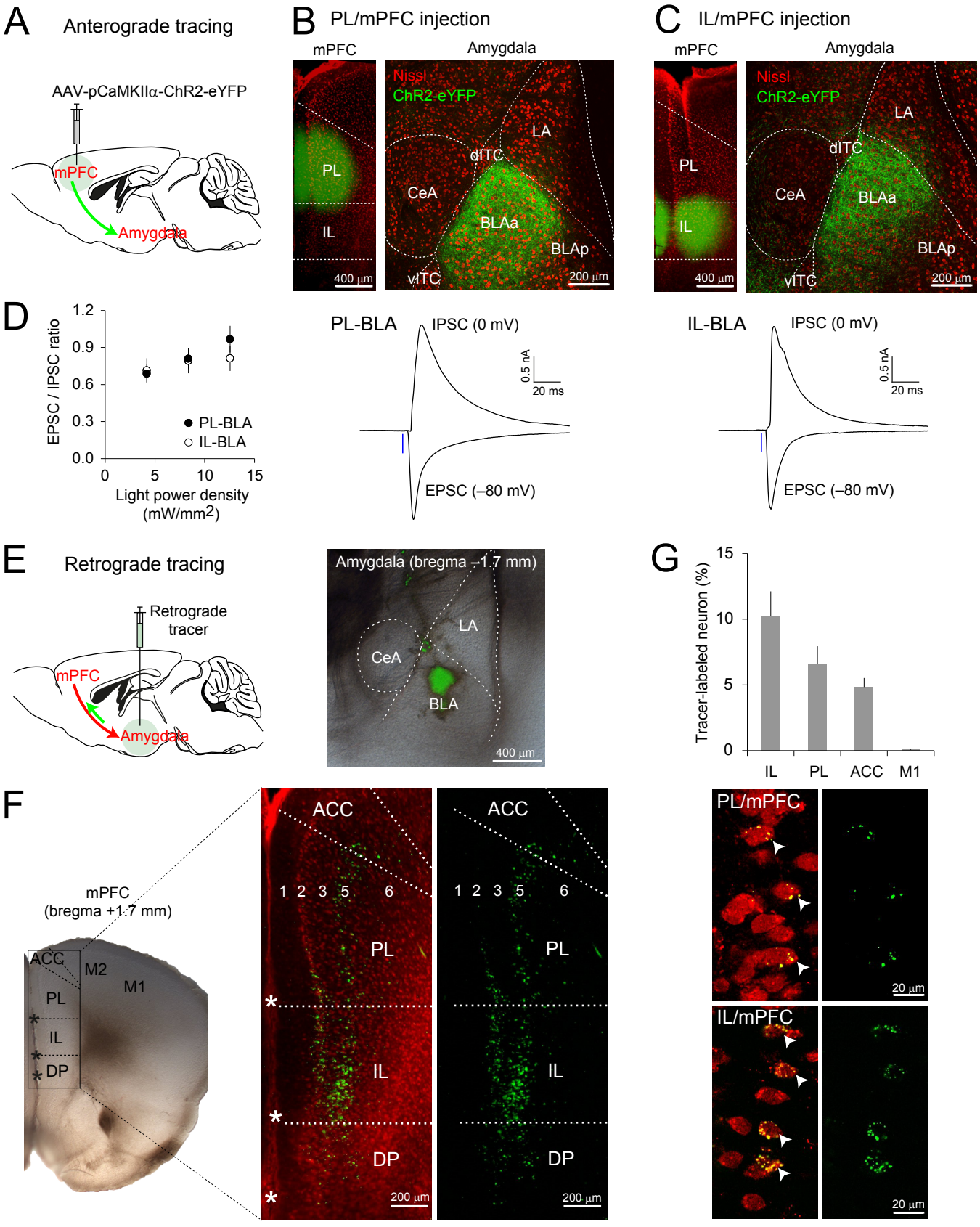
A
Anterograde tracing
AAV-pCaMKIIα-ChR2-eYFP
mPFC
Amygdala
B
PL/mPFC injection
mPFC
Amygdala
Nissl
ChR2-eYFP
PL
IL
LA
dlTC
CeA
BLAa
BLAp
vlTC
400 μm
200 μm
C
IL/mPFC injection
mPFC
Amygdala
Nissl
ChR2-eYFP
PL
IL
LA
dlTC
CeA
BLAa
BLAp
vlTC
400 μm
200 μm
D
EPSC / IPSC ratio
1.2
0.9
0.6
0.3
0.0
0
5
10
15
Light power density
(mW/mm2)
PL-BLA
IL-BLA
PL-BLA
IPSC (0 mV)
0.5 nA
20 ms
EPSC (–80 mV)
IL-BLA
IPSC (0 mV)
0.5 nA
20 ms
EPSC (–80 mV)
E
Retrograde tracing
Retrograde
tracer
mPFC
Amygdala
Amygdala (bregma –1.7 mm)
LA
CeA
BLA
400 μm
G
Tracer-labeled neuron (%)
15
10
5
0
IL
PL
ACC
M1
F
mPFC
(bregma +1.7 mm)
ACC
M2
M1
PL
IL
DP
1 2 3 5 6
ACC
PL
IL
DP
200 μm
PL/mPFC
IL/mPFC
20 μm

Figure S5

Figure S5, related to Figure 1. Anterograde and Retrograde Tracing Studies of the mPFC to Amygdala Pathways

(A) A diagram illustrating stereotaxic injection of ChR2-eYFP-coding AAV into different divisions of the mPFC, sending projections to the amygdala.
(B) Left, a microscopic image showing localized expression of ChR2-eYFP in mice which received AAV injection into the PL (n = 5 mice). Right, an image showing projections from the PL/mPFC (green) in the amygdala, mainly in the anterior division of the BLA (BLAa). Red fluorescence is Nissl stain. LA, lateral nucleus of the amygdala; BLAa and BLAp, anterior and posterior divisions of the basolateral amygdala; dITC and vITC, dorsal and ventral clusters of intercalated neurons, CeA, central nucleus of the amygdala.
(C) Representative images of the mPFC (left) and the amygdala (right) in mice which received localized injection of the AAV-ChR2-eYFP into the IL/mPFC (as in Figure S4, n = 5 mice). Note dense projections from the IL (green) to the BLAa.
(D) Left, summary plot showing average EPSC/IPSC amplitude ratios in PL-BLA (filled symbols) or IL-BLA pathways (open symbols). Middle, representative traces of EPSCs and IPSCs in the BLA in mice which received AAV-ChR2-eYFP injection into the PL/mPFC. Right, EPSCs and IPSCs in the BLA in mice which received AAV-ChR2-eYFP injection into the IL. Monosynaptic EPSCs and disynaptic IPSCs were evoked by photostimulation of projections from the mPFC with three different intensities (4.2, 8.4, and 12.5 mW/mm^2), and recorded in principal neurons of the BLAa in voltage-clamp mode at –80 and at 0 mV, respectively. EPSC/IPSC amplitude ratio was calculated from peak amplitudes of EPSC and IPSC evoked by photostimulation of the same light intensities in each BLA neuron. There was no significant difference in EPSC/IPSC amplitude ratio between PL-BLA and IL-BLA pathways ($p = 0.54$, 16 neurons from 5 mice for PL-BLA pathway, and n = 18 neurons from 5 mice for IL-BLA pathway).
(E) Left, a diagram showing stereotaxic injection of the fluorescent retrograde tracer into the BLA, receiving projections from the mPFC. Right, a microscopic image showing the injection site of the retrograde tracer (green) in the BLA.
(F) Box in the left image indicates the area which is magnified in right panels. Right, a microscopic image showing the distribution of mPFC neurons labeled with retrograde tracer (green) that was injected into the BLA (as in E). Red fluorescence is Nissl stain. Asterisks mark blood vessels between hemispheres, which were used as a guide for locating the PL and the IL in high magnification images. Dotted lines indicate approximate borders between different cortical areas. Numbers within fluorescent images indicate cortical layers. Note retrograde tracer-labeled neurons in both PL and IL of the mPFC. ACC: anterior cingulate cortex, PL and IL: prelimbic and infralimbic divisions of the mPFC, DP: dorsal peduncular cortex.
(G) Top, summary graph showing proportions of retrograde tracer-labeled neurons in different cortical areas in mice which received injections of the retrograde tracer into the BLA (as in E). M1, primary motor cortex. To quantify the density of BLA-projecting neurons in the mPFC, the number of labeled neurons was divided with the total number of cells within the square area (0.34 mm^2) covering cortical layers 1-5. The field of view was centered at the area where labeled neurons were distributed most densely in each cortical area. For each mouse, average density of labeled neurons was calculated from

3 different coronal sections (300 μm apart). Data from 5 mice were averaged to generate this summary plot. Bottom, high-magnification fluorescent images showing retrograde tracer-labeled neurons (arrowheads) in the PL and IL divisions of the mPFC. Red fluorescence is Nissl stain. Multiple green puncta compacted within cell bodies (red) indicate vesicles containing retrograde tracer transported from the BLA. Error bars are SEM.

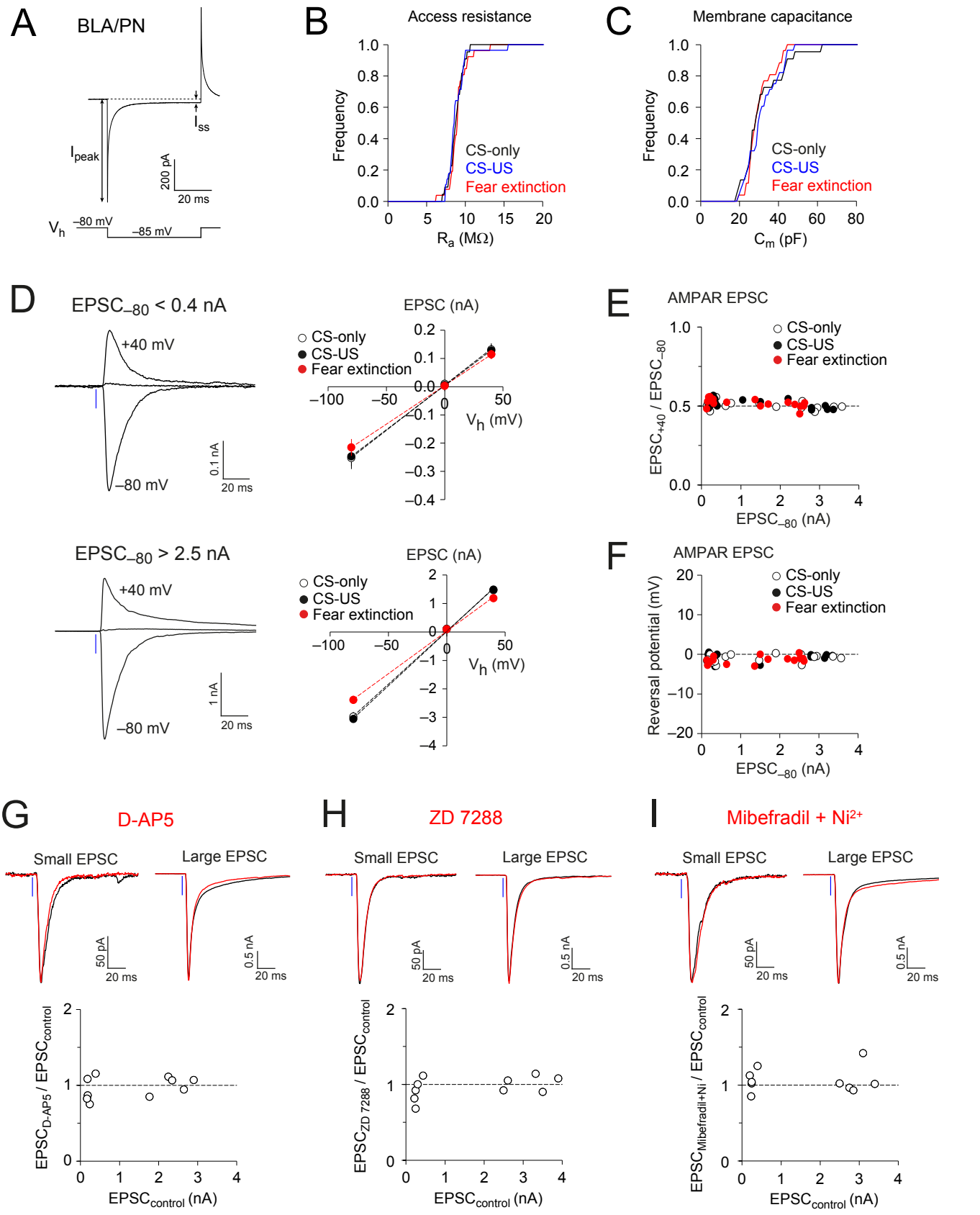
A
BLA/PN
I_{peak}
I_{ss}
200 pA
20 ms
V_h
–80 mV
–85 mV
B
Access resistance
Frequency
CS-only
CS-US
Fear extinction
R_a (MΩ)
C
Membrane capacitance
Frequency
CS-only
CS-US
Fear extinction
C_m (pF)
D
$EPSC_{-80}$ < 0.4 nA
+40 mV
–80 mV
0.1 nA
20 ms
EPSC (nA)
CS-only
CS-US
Fear extinction
V_h (mV)
$EPSC_{-80}$ > 2.5 nA
+40 mV
–80 mV
1 nA
20 ms
EPSC (nA)
CS-only
CS-US
Fear extinction
V_h (mV)
E
AMPAR EPSC
CS-only
CS-US
Fear extinction
$EPSC_{+40}$ / $EPSC_{-80}$
$EPSC_{-80}$ (nA)
F
AMPAR EPSC
CS-only
CS-US
Fear extinction
Reversal potential (mV)
$EPSC_{-80}$ (nA)
G
D-AP5
Small EPSC
Large EPSC
50 pA
20 ms
0.5 nA
20 ms
$EPSC_{D\text{-}AP5}$ / $EPSC_{control}$
$EPSC_{control}$ (nA)
H
ZD 7288
Small EPSC
Large EPSC
50 pA
20 ms
0.5 nA
20 ms
$EPSC_{ZD\ 7288}$ / $EPSC_{control}$
$EPSC_{control}$ (nA)
I
Mibefradil + Ni^{2+}
Small EPSC
Large EPSC
50 pA
20 ms
0.5 nA
20 ms
$EPSC_{Mibefradil+Ni}$ / $EPSC_{control}$
$EPSC_{control}$ (nA)

Figure S6

Figure S6, related to Figure 2. Passive Membrane Properties of BLA principal neurons and Voltage-Clamp Recordings of EPSCs with Large Amplitudes

(A) A trace represents the average of 20 current traces induced by hyperpolarizing voltage pulses (50 ms-long, 5 mV from a holding voltage (V_h) of –80 mV), and recorded in a principal neuron in the BLA (BLA/PN) in voltage-clamp mode with a sampling rate of 100 kHz. Peak amplitude of the transient capacitive current (I_{peak}) was used to estimate apparent access resistance (R_a) using the equation, R_a = –5 mV / I_{peak}. Steady-state current (I_{ss}) is the average current from the baseline for the last 5 ms of voltage pulse. It was used to calculate input resistance (R_{in}) using the equation, R_{in} = (–5 mV / I_{ss}) - R_a. Decay time constant (τ) of capacitive transient was estimated by fitting the curve with a double exponential function, and the fast component of τ in the double exponential fit was used to calculate membrane capacitance (C_m) using the equation, $C_m = \tau \times (R_a + R_{in}) / (R_a \times R_{in})$.
(B and C) Cumulative histograms of access resistance (B), and membrane capacitance (C) in BLA/PN in mice from different behavioral groups (n = 22, 28, and 26 cells from 4, 7, and 6 mice for CS-alone, fear conditioning (CS-US) and fear extinction groups, respectively).
(D) Representative traces of AMPA receptor-mediated EPSCs (AMPAR-EPSC) recorded at holding potentials (V_h) of –80, 0 and +40 mV (left), and summary plots of the current-voltage (I-V) relationships (right). EPSCs were evoked by photostimulation of ChR2-expresing projections from the mPFC, and recorded in BLA/PN in voltage-clamp mode (as in Figures 2G and 2H). Upper panels represent the results of analysis for relatively small AMPAR-EPSCs at –80 mV ($EPSC_{-80}$ < 0.4 nA, n = 3-6 cells per each group) whereas lower panels represent the results of analysis for relatively large $EPSC_{-80}$ (> 2.5 nA, n = 5-6 cells per each group). D-AP5 (50 μM) and bicuculline (30 μM) were added to inhibit synaptic responses mediated by NMDA and $GABA_A$ receptors, respectively. Spermine was not included in pipette solution to prevent possible inward rectification of AMPAR-EPSCs at a positive holding potential. Dotted lines in I-V plots are derived from linear regression of average amplitudes of EPSCs recorded at different holding potentials. Note linear I-V relationship and reversal potential (E_{rev}) close to 0 mV for both small and large $EPSC_{-80}$ in all behavioral groups. In the I-V plot of large $EPSC_{-80}$, error bars were very small so that they were hidden within the symbols (circles).
(E) A plot of the $EPSC_{+40}/EPSC_{-80}$ ratio versus peak amplitudes of $EPSC_{-80}$. A dotted horizontal line indicates expected $EPSC_{+40}/EPSC_{-80}$ ratio (0.5) based on linear I-V relationship and the reversal potential of 0 mV for AMPAR-EPSC.
(F) A plot of E_{rev} of AMPAR EPSC versus peak amplitudes of $EPSC_{-80}$. No significant correlation between E_{rev} and $EPSC_{-80}$ was detected (r = 0.28, p = 0.30). E_{rev} of AMPAR EPSC was calculated in each recorded neuron from linear regression of peak amplitudes of EPSCs recorded at –80, 0 and +40 mV as in D.
(G) Top, representative traces of small (left) and large EPSCs (right) in the mPFC-BLA pathway in the absence (black) and presence of the NMDA receptor inhibitor (50 μM D-AP5, red). EPSCs were recorded in BLA/PN at –80 mV as in D. Small and large EPSCs were defined as baseline EPSCs with peak amplitudes of < 0.4 nA and > 2.0 nA, respectively. The effect of D-AP5 was estimated for both small and large EPSCs in the same neuron. The ratio of peak amplitudes of EPSCs recorded in the presence of D-

AP5 to baseline EPSC ($EPSC_{D\text{-}AP5}/EPSC_{control}$) was calculated in each neuron. Bottom, a summary plot of $EPSC_{D\text{-}AP5}/EPSC_{control}$ ratio versus $EPSC_{control}$ (n = 5 neurons). A dotted line indicates $EPSC_{D\text{-}AP5}/EPSC_{control} = 1$.

(H) Same as in (G), but 10 μM ZD 7288 was applied in these experiments to inhibit hyperpolarization-activated cyclic nucleotide-gated channels (n = 5 neurons).

(I) Same as in (G), but 10 μM mibefradil and 10 μM Ni^{2+} were applied to inhibit T-type and R-type voltage-dependent Ca^{2+} channels (n = 5 neurons). Error bars are SEM.

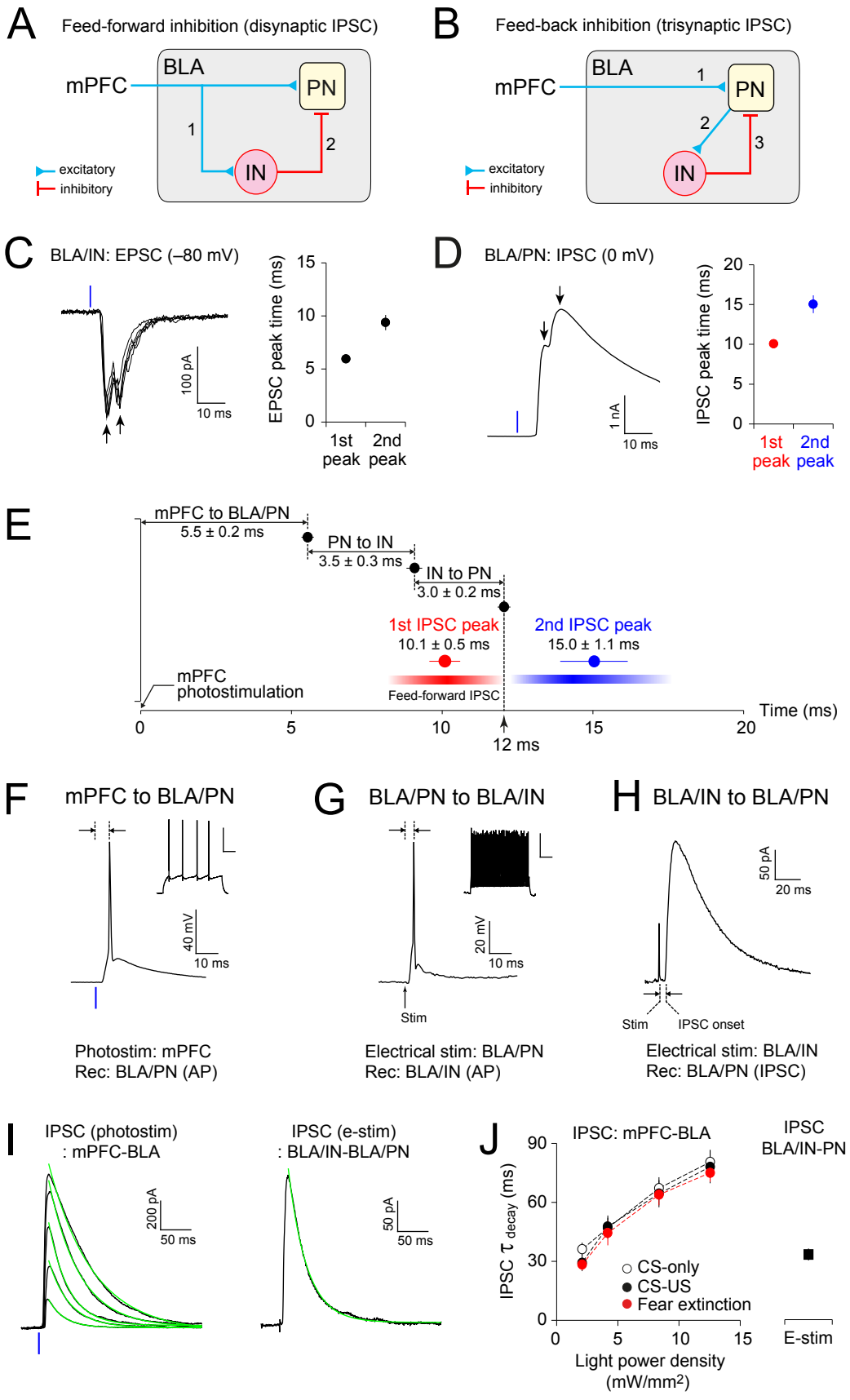
A
Feed-forward inhibition (disynaptic IPSC)
mPFC
BLA
PN
IN
1
2
excitatory
inhibitory
B
Feed-back inhibition (trisynaptic IPSC)
mPFC
BLA
PN
IN
1
2
3
excitatory
inhibitory
C
BLA/IN: EPSC (–80 mV)
100 pA
10 ms
EPSC peak time (ms)
15
10
5
0
1st peak
2nd peak
D
BLA/PN: IPSC (0 mV)
1 nA
10 ms
IPSC peak time (ms)
20
15
10
5
0
1st peak
2nd peak
E
mPFC to BLA/PN
5.5 ± 0.2 ms
PN to IN
3.5 ± 0.3 ms
IN to PN
3.0 ± 0.2 ms
1st IPSC peak
10.1 ± 0.5 ms
2nd IPSC peak
15.0 ± 1.1 ms
mPFC photostimulation
Feed-forward IPSC
Time (ms)
0
5
10
15
20
12 ms
F
mPFC to BLA/PN
40 mV
10 ms
Photostim: mPFC
Rec: BLA/PN (AP)
G
BLA/PN to BLA/IN
20 mV
10 ms
Stim
Electrical stim: BLA/PN
Rec: BLA/IN (AP)
H
BLA/IN to BLA/PN
50 pA
20 ms
Stim
IPSC onset
Electrical stim: BLA/IN
Rec: BLA/PN (IPSC)
I
IPSC (photostim)
: mPFC-BLA
200 pA
50 ms
IPSC (e-stim)
: BLA/IN-BLA/PN
50 pA
50 ms
J
IPSC: mPFC-BLA
IPSC τ decay (ms)
90
60
30
0
CS-only
CS-US
Fear extinction
0
5
10
15
Light power density
(mW/mm2)
IPSC
BLA/IN-PN
E-stim

Figure S7

Figure S7, related to Figures 4 and 5. Feed-Forward and Feed-Back Inhibition in the mPFC-BLA Pathway

(A and B) Diagrams showing neural circuits of feed-forward (A) and feed-back inhibition (B) of principal neurons in the BLA (BLA/PN) by projections from the mPFC. Numbers within the diagrams indicate the order of activation (AP firing) in excitatory (blue) or inhibitory projections (red). IN, local inhibitory interneurons in the BLA.
(C) Left, superimposed EPSCs recorded in an inhibitory interneuron in the BLA. Blue vertical line indicates photostimulation of the mPFC projections. Note double EPSC peaks (arrows). Right, summary plot showing average latencies to the first and second peaks from the start of photostimulation (n = 5 neurons from 5 mice).
(D) Left, the representative IPSC with double peaks (arrows) recorded in a principal neuron in the BLA. Blue vertical line indicates photostimulation of projections from mPFC. Right, summary plot indicating average latencies to the first and second IPSC peaks from the start of photostimulation (n = 5 neurons from 4 mice).
(E) Estimation of latency of feed-back inhibition in the mPFC-BLA pathway. Average delays of each component of the feed-back circuit were calculated from experiments described in panels F-H. We estimated the IPSC latency (~12 ms) in feed-back inhibitory circuit by adding average delays in each component. Based on these estimates, we set the window of 8.0-12.0 ms from the onset of photostimulation to detect peak amplitudes of feed-forward IPSCs in BLA/PN. The first IPSC peaks in (D) (red) likely reflected feed-forward IPSCs with little contamination of feed-back IPSCs since their average time to peak (10.1 ± 0.5 ms) was smaller than the estimated latency of feed-back inhibition (~12 ms). The second IPSC peak in (D) (blue, average peak time of 15.0 ± 1.1 ms) may reflect feed-back or more complex polysynaptic IPSCs.
(F) A representative trace of AP firing induced by photostimulation of mPFC projections at the maximum intensity (12.5 mW/mm^2, 1 ms long, blue vertical line), and recorded in a BLA/PN at resting membrane potential in current-clamp mode. For each BLA/PN, the latency of the earliest AP firing from the onset of photostimulation was measured (arrows) to estimate the minimal latency of AP firing in BLA/PN. K^+-based pipette solution was used to verify the cell type of recorded neurons based on AP firing pattern during 1 s-long current injections (inset, scale bar: 0.2 s, 40 mV). n = 12 neurons.
(G) A representative trace of AP firings recorded in an interneuron of the BLA (BLA/IN) at resting membrane potential in current-clamp mode. Principal neurons of the BLA (BLA/PN) were stimulated with an electrode placed onto the BLA near the recorded interneuron. The time of electrical stimulation is indicated by a vertical arrow (Stim). To measure the minimal latency of AP firings in the BLA/PN-BLA/IN pathway, the BLA was stimulated electrically with the maximum intensity just below the level directly inducing AP firing in the recorded interneuron. K^+-based pipette solution was used to verify the cell type of recorded neurons based on AP firing pattern during 1 s-long current injection (inset, scale bar: 0.2 s, 40 mV). n = 11 cells.
(H) An IPSC trace recorded in a BLA/PN at 0 mV in voltage-clamp mode as in Figures 5H-5K. BLA/IN were stimulated with an electrode placed onto the BLA in the presence of 10 μM NBQX + 50 μM D-AP5. For each BLA/PN, the shortest latency from stimulation (Stim) to IPSC onset was measured to estimate the minimal latency of IPSCs in the BLA/IN-BLA/PN pathway. n = 13 neurons.

(I) Representative traces of IPSCs in the mPFC-BLA (left) and BLA/IN-BLA/PN pathways (right) for analyses of decay time constant. IPSCs in the mPFC-BLA pathway were induced by photostimulation of mPFC projections with different intensities as in 5L-5N. Monosynaptic IPSCs in the BLA/IN-BLA/PN were evoked electrically in the presence of 10 μM NBQX + 50 μM D-AP5 as in Figures 5H-5K. IPSCs were recorded at 0 mV in BLA/PN in voltage-clamp mode. Cs^+-based pipette solution containing high [Cl^-] (132 mM) was used. Decay phase of IPSCs was fit to the single exponential function (overlaid as green curves) to calculate decay time constant.

(J) A summary plot of decay time constant (τ_{decay}) of IPSCs in the mPFC-BLA (left, open symbols) and BLA/IN-BLA/PN pathways (right, square symbol). Decay time constant of IPSCs in the mPFC-BLA pathway at low photostimulation intensity (2 mW/mm^2) was similar to that of monosynaptic IPSCs in the BLA/IN-BLA/PN pathway ($p = 1.00$). At higher intensities (4, 8 and 12.5 mW/mm^2), however, decay time constants in the mPFC-BLA pathway were significantly larger compared to that in the BLA/IN-BLA/PN pathway ($p < 0.05$). There was no significant difference in decay time constant of IPSCs in the mPFC-BLA pathway between behavioral groups ($p = 0.49$). The data set in Figures 5M and 5N was used for analysis of decay kinetics of IPSCs in the mPFC-BLA pathway. Error bars are SEM.

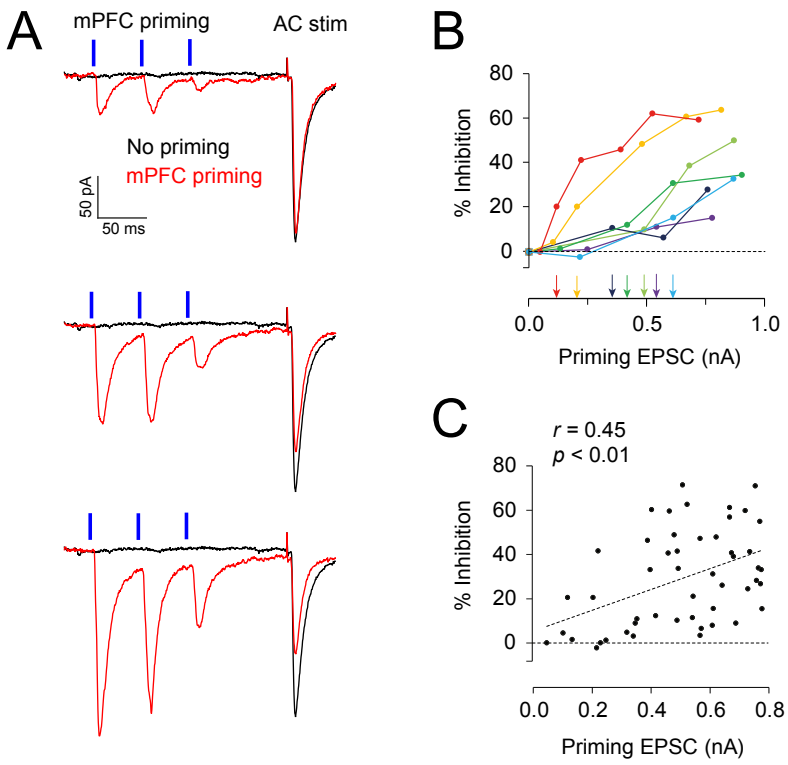
A
mPFC priming
AC stim
No priming
mPFC priming
50 pA
50 ms
B
% Inhibition
80
60
40
20
0
0.0
0.5
1.0
Priming EPSC (nA)
C
r = 0.45
p < 0.01
% Inhibition
80
60
40
20
0
0.0
0.2
0.4
0.6
0.8
Priming EPSC (nA)

Figure S8

Figure S8, related to Figure 6. Threshold of mPFC Priming for the Induction of Heterosynaptic Inhibition in Auditory Cortical Inputs to the BLA

(A) Traces illustrating heterosynaptic inhibition of EPSCs in the auditory cortex (AC)-to-BLA pathway induced by priming photostimulation of mPFC projections with different light intensities in the same BLA principal neuron (BLA/PN). Three pulses of photostimulation (1 ms duration, 50 ms inter-pulse interval, blue vertical lines) with increasing intensity from the top to the bottom were applied to projections from the mPFC (mPFC priming). The AC-BLA pathway was stimulated electrically (AC stim) 200 ms after the first photostimulation. Note significant heterosynaptic inhibition of the EPSC in the AC-BLA pathway (red traces) in the middle and lower recordings compared to no priming control (black traces).
(B) Summary plot showing dependence of the magnitude of heterosynaptic inhibition of the EPSCs in the AC-BLA pathway on priming EPSC amplitude (the mPFC-BLA pathway). Results from different neurons are plotted with different colors (n = 7 neurons from 3 mice). The magnitude of heterosynaptic inhibition was quantified as percentage of the baseline EPSC recorded without mPFC priming (% inhibition). Arrows at x-axis indicate the threshold of mPFC activation at which heterosynaptic inhibition could be induced. It was estimated as the smallest priming EPSC, at which significant heterosynaptic inhibition (>10 % inhibition) was induced in each BLA/PN tested.
(C) Scatter plot showing the magnitude of heterosynaptic inhibition as a function of the priming EPSC amplitude (r = 0.45, $p < 0.01$). Data from different neurons were pulled together.

Supplemental Tables

Table S1. Summary of statistical analysis (ANOVA)

Data	ANOVA	Response variable	Factors	DF	F value	P value
Figure 2C	One-way	Pre-CS freezing	Behavioral groups	(2, 55)	0.09	0.914
Figure 2C	One-way	Freezing to the CS	Behavioral groups	(2, 55)	52.21	< 0.001
			* Post-hoc comparison: P < 0.0001, CS-US vs CS-only or extinction			
Figure 2E	One-way	Resting membrane potential	Behavioral groups	(2, 53)	0.69	0.508
Figure 2E	One-way	Input resistance	Behavioral groups	(2, 56)	0.80	0.453
Figure 2F	Two-way	AP frequency	Behavioral groups	(2, 454)	2.81	0.061
			Injected current	(7, 454)	113.53	< 0.001
			Interaction	(14, 454)	0.11	1.000
Figure 2H	Two-way	EPSC peak amplitude	Behavioral groups	(2, 774)	14.00	< 0.001
			Light power density	(4, 774)	198.33	< 0.001
			Interaction	(8, 774)	0.81	0.600
			* Post-hoc comparison: P < 0.0001, extinction vs CS-only or CS-US			
Figure 2K	Two-way	AP probability	Behavioral groups	(2, 163)	6.47	0.002
			Light power density	(4, 163)	73.76	< 0.001
			Interaction	(8, 163)	1.84	0.073
			* Post-hoc comparison: P < 0.05 or 0.01, extinction vs CS-only or CS-US			
Figure 2L	Two-way	AP latency	Behavioral groups	(2, 149)	13.35	< 0.001
			Light power density	(5, 149)	16.07	< 0.001
			Interaction	(10, 149)	0.86	0.572
			* Post-hoc comparison: P < 0.0001, extinction vs CS-US or CS-only			
Figure 3B	Two-way	Paired-pulse ratio (PPR)	Behavioral groups	(2, 172)	6.45	0.002
			Light power density	(3, 172)	20.55	< 0.001
			Interaction	(6, 172)	0.25	0.958
			* Post-hoc comparison: P < 0.05 or 0.01, extinction vs CS-only or CS-US			
Figure 3D	Two-way	AMPAR EPSC (normalized)	Behavioral groups	(2, 401)	1.04	0.356
			Holding potential	(6, 401)	451.29	< 0.001
			Interaction	(12, 401)	0.21	0.998
Figure 3D	Two-way	NMDAR EPSC (normalized)	Behavioral groups	(2, 409)	0.03	0.966
			Holding potential	(6, 409)	310.33	< 0.001
			Interaction	(12, 409)	0.39	0.965
Figure 3E	One-way	AMPA/NMDA raio	Behavioral groups	(2, 61)	0.51	0.604
Figure 4H	One-way	Synaptic latency	Group (mPFC-EPSC/IPSC, AC-EPSC)	(2, 59)	125.55	< 0.001
			* Post-hoc comparison: P < 0.0001, mPFC-IPSC vs mPFC-EPSC or AC-EPSC			
Figure 5B	One-way	Resting membrane potential	Behavioral groups	(2, 79)	0.14	0.872
Figure 5B	One-way	Input resistance	Behavioral groups	(2, 69)	2.83	0.066
Figure 5C	Two-way	AP frequency	Behavioral groups	(2, 397)	1.38	0.253
			Injected current	(4, 397)	38.20	< 0.001
			Interaction	(8, 397)	0.14	0.997
Figure 5E	Two-way	EPSC peak amplitude	Behavioral groups	(2, 275)	0.87	0.421
			Light power density	(4, 275)	28.04	< 0.001
			Interaction	(8, 275)	0.06	1.000
Figure 5G	Two-way	AP probability	Behavioral groups	(2, 131)	0.74	0.479
			Light power density	(3, 131)	43.38	< 0.001
			Interaction	(6, 131)	0.34	0.913
Figure 5I	One-way	Reversal potential	Behavioral groups	(2, 28)	1.38	0.269
Figure 5K	Two-way	IPSC peak amplitude	Behavioral groups	(2, 368)	1.07	0.344
			Light power density	(7, 368)	55.38	< 0.001
			Interaction	(14, 368)	0.10	1.000
Figure 5N	Two-way	Feed-forward IPSC	Behavioral groups	(2, 172)	0.69	0.501
			Light power density	(3, 172)	45.30	< 0.001
			Interaction	(6, 172)	0.14	0.991
Figure 5N	One-way	IPSC amplitude/weak stim	Behavioral groups	(2, 41)	0.02	0.980
Figure 6J	Two-way	EPSC Inhibition (%)	CGP (no priming vs mPFC priming)	(1, 35)	3.23	0.081
			Time interval (Δt)	(3, 35)	0.39	0.761
			Interaction	(3, 35)	0.39	0.761

Table S1. (continued)

Data	ANOVA	Response variable	Factors	DF	F value	P value
Figure 6J	Two-way	EPSC Inhibition (%)	Group (control vs CGP 52432)	(1, 35)	46.58	< 0.001
			Time interval (Δt)	(3, 35)	15.62	< 0.001
			Interaction	(3, 35)	10.89	< 0.001
Figure 6K	Two-way	PPR (normalized)	CGP (no priming vs mPFC priming)	(1, 35)	0.08	0.775
			Time interval (Δt)	(3, 35)	0.59	0.627
			Interaction	(3, 35)	0.59	0.627
Figure 6K	Two-way	PPR (normalized)	Group (control vs CGP 52432)	(1, 35)	27.18	< 0.001
			Time interval (Δt)	(3, 35)	5.35	0.004
			Interaction	(3, 35)	3.81	0.018
Figure 6M	Two-way	EPSC Inhibition (%)	Behavioral groups	(2, 191)	11.41	< 0.001
			Time interval (Δt)	(3, 191)	38.53	< 0.001
			Interaction	(6, 191)	1.18	0.317
			* Post-hoc comparison: P < 0.001 or 0.05, extinction vs CS-only or CS-US			
Figure 6N	Two-way	PPR (normalized)	Behavioral groups	(2, 190)	6.66	0.002
			Time interval (Δt)	(3, 190)	19.12	< 0.001
			Interaction	(6, 190)	0.95	0.462
			* Post-hoc comparison: P < 0.01 or 0.05, extinction vs CS-only or CS-US			
Figure 7B	One-way	EPSC latency	Group (BLA/PN, dITC, vITC)	(2, 45)	0.04	0.960
Figure 7D	Two-way	EPSC amplitude (dorsal ITC)	Behavioral groups	(2, 344)	0.55	0.578
			Light power density	(4, 344)	26.48	< 0.001
			Interaction	(8, 344)	0.13	0.998
Figure 7D	Two-way	EPSC amplitude (ventral ITC)	Behavioral groups	(2, 102)	0.02	0.978
			Light power density	(4, 102)	6.81	< 0.001
			Interaction	(8, 102)	0.01	1.000
Figure 7F	Two-way	AMPAR EPSC (normalized)	Behavioral groups	(2, 215)	0.17	0.846
			Holding potential	(6, 215)	102.69	< 0.001
			Interaction	(12, 215)	0.10	1.000
Figure 7F	Two-way	NMDAR EPSC (normalized)	Behavioral groups	(2, 264)	0.01	0.992
			Holding potential	(6, 264)	88.59	< 0.001
			Interaction	(12, 264)	0.21	0.998
Figure 7G	One-way	AMPA/NMDA raio	Behavioral groups	(2, 25)	0.03	0.973
Figure 7J	One-way	EPSC/IPSC ratio	Group (BLA/PN, ITC, CeM)	(2, 46)	21.26	< 0.001
			* Post-hoc comparison: P < 0.0001 or 0.01, CeM vs BLA/PN or ITC			
Figure S2G	One-way	EPSC latency	Behavioral groups	(2, 113)	1.75	0.178
Figure S2G	One-way	IPSC latency	Behavioral groups	(2, 77)	0.22	0.803
Figure S2J	One-way	EPSC latency	Group (LA, BLA, ITC, CeL, CeM)	(4, 77)	0.19	0.942
Figure S2J	One-way	IPSC latency	Group (LA, BLA, ITC, CeL, CeM)	(4, 77)	13.79	< 0.001
			* Post-hoc comparison: P < 0.05, CeM vs LA, BLA, ITC or CeL			
Figure S3I	One-way	EPSC peak amplitude	Light power density	(3, 206)	29.50	< 0.001
Figure S3I	One-way	EPSC tau decay	Light power density	(3, 84)	0.36	0.782
Figure S3I	One-way	EPSC tau decay	Group (control vs TTX+4AP)	(4, 93)	0.95	0.438
			* Post-hoc comparison: P > 0.784, control vs TTX+4-AP			
Figure S5D	Two-way	EPSC/IPSC ratio	Group (PL-BLA vs IL-BLA)	(1, 89)	0.38	0.538
			Light power density	(2, 89)	1.93	0.151
			Interaction	(2, 89)	0.51	0.603
Figure S5G	One-way	Labeled neuron (%)	Group (IL, PL, ACC, M1)	(3, 24)	8.26	0.001
			* Post-hoc comparison: P = 0.336, PL vs IL			
Figure S6B	One-way	Access resistance	Behavioral groups	(2, 73)	0.19	0.827
Figure S6C	One-way	Membrane capacitance	Behavioral groups	(2, 73)	0.21	0.811
Figure S7J	Two-way	IPSC tau decay	Behavioral groups	(2, 117)	0.72	0.490
			Light power density	(3, 117)	37.36	< 0.001
			Interaction	(6, 117)	0.09	0.997
Figure S7J	One-way	IPSC tau decay	Group (strong photostim vs E-stim)	(3, 100)	4.73	0.004
			* Post-hoc comparison: P < 0.05, strong photostim vs E-stim			
Figure S7J	One-way	IPSC tau decay	Group (weak photostim vs E-stim)	(3, 37)	1.46	0.240
			* Post-hoc comparison: P = 1.00, weak photostim vs E-stim			

Table S2. Summary of statistical analysis (Student's t-test)

Data	t-test	Response variable	Groups	P value	
Figure 3H	Unpaired	EPSC (% baseline)	Control vs BAPTA	0.017	
Figure 3J	Paired	Paired-pulse ratio	Baseline vs LTD	0.029	
Figure 4I	Paired	Charge transfer	Control vs bicuculline	0.021	
Figure 4I	Paired	EPSC decay time	Control vs bicuculline	0.006	
Figure 6E	Paired	EPSC peak amplitude	No priming vs mPFC priming	< 0.001	For $\Delta t \leq 0.8$ s
Figure 6F	Paired	Paired-pulse ratio	No priming vs mPFC priming	< 0.001	For $\Delta t \leq 0.8$ s
Figure 7I	Unpaired	Synaptic latency	EPSC vs IPSC	< 0.001	
Figure S3C	Paired	EPSC (% baseline)	TTX vs TTX+4-AP	< 0.001	
Figure S3C	Paired	EPSC tau decay	Control vs TTX+4AP	0.288	
Figure S6G	Paired	EPSC peak amplitude	Control vs D-AP5	0.883	
Figure S6H	Paired	EPSC peak amplitude	Control vs ZD 7288	0.709	
Figure S6I	Paired	EPSC peak amplitude	Control vs Mibefradil/Ni	0.364	

Supplemental Experimental Procedures

Stereotaxic surgery and viral injections

Four week-old male C57BL/6 mice (Charles River Laboratory) were used for stereotaxic viral injections. Prior to surgery, mice were anesthetized with a mixture of ketamine and xylazine (160 mg/kg and 12 mg/kg body weight, respectively, intramuscular injection, Sigma-Aldrich), and were checked for the absence of tail-pinch reflex as a sign of sufficient anesthesia. Mice were immobilized in a stereotaxic frame with non-rupture ear bars (David Kopf Instruments), and ophthalmic ointment was applied to prevent eye drying. After midline scalp incision, small bilateral craniotomy was made with a microdrill with 0.5 mm burrs targeting the infralimbic division of the medial prefrontal cortex (IL/mPFC) with stereotaxic coordinates (1.7 mm rostral to bregma, ± 0.4 mm lateral to midline, and 2.6 mm ventral to bregma; Franklin and Paxinos, 2008). For injections into the PL, the coordinates were: 1.7 mm rostral to bregma, ± 0.4 mm lateral to midline, and 1.7 mm ventral to bregma. Glass capillaries with the tip size of 30 μm in outer diameter were loaded with high-titer adeno-associated virus (AAV) carrying CaMKIIα promoter and channelrhodopsin-2(H134R)-eYFP fusion gene (2-5×10^{12} viral particles/mL, serotype 5, packaged by the vector core facility at the University of North Carolina). After placing the tip of the capillary in the IL/mPFC, virus-containing solution was injected into both sides of the IL/mPFC (0.4-0.5 μL per side) using a 10 μL Hamilton microsyringe and a syringe pump at a rate of 0.1 μL/minute. For more localized IL targeting (Figures S4 and S5C), the virus-containing solution (0.2-0.25 μL per side) was injected with 30 degree angle relative to the dorsoventral axis. For localized PL targeting (Figure S5B), the virus-containing solution (0.2-0.25 μL per side) was injected

with a straight angle as potential backflow did not contaminate the IL located oppositely to the direction of injection pipette withdrawal. After injection, the capillary was left in place for additional 5 min to allow diffusion of the virus solution and then withdrawn. The scalp incision was closed with surgical suture, and mice were given ketoprofen-containing saline (~1 mL, 5 mg ketoprofen per kg body weight, subcutaneous injection) for postoperative analgesia and hydration. All animal procedures in this study were approved by the Institutional Animal Care and Use Committee of McLean Hospital.

Electrophysiology

Input-output curves of synaptic responses were obtained from graded EPSCs induced by photostimuli of increasing intensity (0.8, 2.1, 4.2, 8.4 and 12.5 mW/mm^2) and recorded in voltage-clamp mode at –80 mV (Figures 2G-2H, 5D-5E, and 7C-7D). Paired pulse ratio (PPR) of EPSCs was calculated from EPSCs evoked by paired photostimuli (a 50-ms interpulse interval, 1 ms-long) with light intensities of 1.3, 1.7, 2.1 and 2.5 mW/mm^2 (Figure 3A-3B). Since ChR2-mediated photocurrents in IL/mPFC neurons displayed paired-pulse modulation, which depended on photostimulation intensity ($P < 0.001$), photostimulation intensity was chosen carefully in these experiments so that the same paired photostimuli induced double peaks of the photocurrents with similar amplitudes. Synaptic latency was calculated as a time interval between the start of photostimulation and the onset of EPSC or IPSC (Figures 4H, 7B, S2, and S7H). To stimulate the auditory cortical inputs to the BLA (Figures 6, S3E, and S8) or neurons in the BLA (Figures 5H-5K, and S7G-S7H), metal bipolar stimulation electrodes with a 115 μm spacing (MX21AES, FHC) were placed onto the external

capsule or the BLA, respectively, and square current pulses with 100 μs duration were delivered using Master-8 Pulse Stimulator (A.M.P.I.). Reagents were prepared as stock solutions in water at 1000-fold concentrations, and stored at –20°C. Reagents were purchased from Tocris Bioscience (NBQX, D-AP5, tetrodotoxin, CGP 52432, QX 314, 4-aminopyridine, biocytin, ZD 7288, and mibefradil) or Sigma-Aldrich (ATP, GTP, spermine, bicuculline methochloride, and BAPTA).

Photostimulation

Intensity and duration of photostimulation were controlled using pulse stimulator or patch-clamp amplifier. Light power (mW) was measured at 470 nm using a power meter (Coherent) placed under the objective lens, and light power density (mW/mm^2) was calculated by dividing light power by illumination area.

Verification of local GABAergic interneurons in the BLA

In experiments described in Figures 4A-4C, 5A-5G, S3F, S7C and S7G, postsynaptic responses or AP firings were recorded in GABAergic interneurons in the BLA (BLA/IN) using K^+-based pipette solution. For recordings in BLA/IN, we selected cells in the BLA with small round soma (< 10 μm in diameter) and lesser dendritic branching, and verified BLA/IN based on the following electrophysiological properties and responses to photostimulation of ChR2-expressing mPFC. During 1 s-long current injections in current-clamp mode, BLA/IN typically displayed non-accommodating AP firings (Figure 4B), which were much more frequent than in principal neurons in the BLA (BLA/PN, Figures 2F and 5C). The magnitude of afterhyperpolarization was much larger in BLA/IN

than in BLA/PN. Moreover, BLA/IN had larger input resistance (Figure 2E and 5B), and smaller membrane time constant and membrane capacitance than BLA/PN. Compared to BLA/PN, BLA/IN displayed much smaller EPSCs with much faster rise and decay kinetics (Figures 2G and 2H, 5D and 5E, and S7C) and often with multiple peaks (Figure S7C) when projections from the mPFC were photostimulated. Finally, AP firing in BLA/IN required much larger intensity of photostimulation of mPFC projections than in BLA/PN (Figures 2J and 2K, 5F and 5G).

Histology and microscopy

After electrophysiological recordings, slices were fixed in 4% paraformaldehyde-containing phosphate-buffered saline (PBS, 137 mM NaCl, 2.7 mM KCl, 11.9 mM phosphate, pH7.4) at 4°C overnight. After fixation, slices were washed in PBS at room temperature for 15 min, and permeabilized in PBS containing 0.1% Triton X-100 for additional 30 min. Slices were washed again in PBS, and then mounted onto the slide glass. Slices were incubated with Neurotrace Fluoresent Nissl stain (diluted 40-fold in PBS, 615 nm emission wavelength, Molecular Probes) for an hour at room temperature. After fluorescent Nissl staining, slices were washed with PBS and with 0.1% triton X-100-containing PBS for 15 min each. After final wash with PBS for 2 hours, Vectashieled mounting media with DAPI (Vector Laboratories) was applied onto slices, which were then covered with coverslips. Images for Nissl stain (red fluorescence) and ChR2-eYFP (green fluorescence) were captured using Leica TCS SP8 Confocal System (Leica) or Axioskop 2 fluorescent microscope (Carl Zeiss). Images captured with different fluorescent channels were merged using ImageJ software (NIH). For each

mouse, a virus injection site was verified by identifying ChR2-eYFP expression in the mPFC. Mice in which the target area was missed were excluded from the analysis.

Retrograde tracing

For retrograde tracing (Figure S5E-S5G), retrograde tracer solution was prepared by diluting FluoSpheres fluorescent microspheres (0.04 μm diameter, 5 % solid, yellow-green; Molecular Probes) with the equal volume of PBS. Two-month old mice were used for injection of retrograde tracer into the BLA. Stereotaxic coordinates of the BLA were 1.5 mm caudal to the bregma, ±3.2 mm lateral to midline, and 4.8 mm ventral to the bregma. Using micro-syringe pump, 0.3-0.5 μL of the retrograde tracer solution was injected into the BLA at the rate of 0.1 μL per minute. Volume of solid component from tracer solution injected into the BLA was 0.0075-0.0125 μL. Seven days after injection of retrograde tracer, coronal sections of the brain (300 μm thick) were cut using vibratome, and were fixed with 4 % paraformaldehyde overnight. After fluorescent Nissl stain (see Experimental Procedures), injection site in the amygdala and the distribution of labeled neurons in the mPFC were evaluated under Leica TSC SP8 confocal microscope. To quantify the density of BLA-projecting neurons, we captured microscopic images centered at the area where retrograde tracer-labeled neurons were distributed most densely within each cortical area, and calculated the ratio of the number of labeled neurons to the total number of Nissl-stained cells within the field of view (~500 cells). The area of the field covering cortical layer 1 to 5 was 0.34 mm^2. Retrograde tracer-labeled neurons were defined as cells with multiple green puncta, which colocalize with Nissl-stained cell bodies (red), and were identified by visual

inspection. Total number of cells within the field was calculated using ImageJ software. The proportion of labeled neurons calculated from 3 different coronal sections (300 μm apart) was averaged for each mouse. Mice where retrograde tracer injection missed the target (the BLA) were excluded from the analysis.

Morphological identification of recorded neurons

In some experiments (Figure S1A-S1E), recorded neurons in the amygdala were loaded with the Cs-methanesulfonate-based pipette solution containing 5 mM biocytin (Tocris) for 20 minutes. After loading biocytin, pipette was withdrawn slowly, and brain slices were fixed overnight with 4 % paraformaldehyde. After washing slices with PBS containing 0.2% Triton X-100 twice for 15 min each, they were incubated with streptavidin, Alexa 568 conjugate (20 μg/mL in PBS, Molecular Probes) for 2 hours at room temperature. Then, unbound streptavidin was washed out with PBS three times for 20 min each, and slices were mounted onto slides. Images of labeled neurons were taken using Leica TSC SP8 confocal microscope, and neuronal morphology and location within the amygdala were analyzed.

Control of experimental variability

Several factors were affecting ChR2 expression and photostimulation-induced synaptic responses in the amygdala. Extra precautions were taken to control for these variables in order to increase the statistical power of experimental analysis, permitting a detection of changes associated with behavioral training. To maximize viral transduction efficiency in mPFC neurons and obtain robust synaptic responses in the amygdala, AAV-ChR2-

eYFP was used in high titer of at least $2x10^{12}$/mL ($4\text{-}5x10^{12}$/mL in most experiments). Although AAV vectors were always from the same facility (Vector Core Facility at the University of North Carolina), the AAV titer of virus varied slightly between different batches (or lots) of AAV. Thus, the volume of AAV injected into the mPFC was adjusted, so that the amount of viral particles was consistent. Furthermore, AAV injections and behavioral training were performed on the age- and gender-matched mice. At the age P28, stereotaxic surgeries for bilateral AAV injections were performed on a cohort of three C57BL/6 littermate male mice on the same experimental day. Surgical procedures were standardized to minimize the variability of AAV injections, using the same stereotaxic coordinates for the mPFC and the same amount of AAV injected into the mPFC for all mice. Four weeks after the surgery, mice in the same cohort were randomly assigned to each of three groups, including CS-only, CS-US (fear conditioning), and fear extinction groups, for subsequent behavioral training. This grouping method was efficient in reducing experimental variability. In some cases, one of three mice was assigned to naive group instead of CS-only group, and used for control experiments not involving behavioral training (e.g., for connectivity studies). Two mice in extinction group failed to recall extinction memory (with freezing time >80 % on day 3), and they were excluded from analysis.

For each mouse, electrophysiological recordings in slices were performed immediately after the freezing test on day 3. On a recording day, when mice were approximately 8 week-old, we prepared only three coronal brain slices (300 μm thick) per hemisphere, containing the amygdala with projections from the mPFC. After preparing slices, the extent and intensity of GFP signal was examined in the mPFC and

the amygdala to verify that ChR2 expression was consistent in mice from different groups. When GFP signal in the mPFC or amygdala was much weaker on one side of the brain than on the other side, we did not collect data from that hemisphere, assuming that AAV was not injected well (e.g., due to clogging of injection pipette or backflow/leakage toward the pial surface). This happened once in CS-only and fear extinction groups. Since the BLA in rostral slices received denser mPFC projections than in more caudally-located slices, synaptic responses (EPSCs or IPSCs) were recorded from only one neuron located near the center of the anterior division of the BLA per slice in experiments comparing the input-output curves between different behavioral groups. Thus, synaptic responses were recorded from the total of 4-6 BLA neurons per mouse. We chose principal neurons with relatively large soma (> 20 μm in diameter) in anterior division of the BLA to get robust synaptic responses and to reduce variability between groups. To minimize the variability due to potential voltage errors in voltage-clamp recordings, access resistance was kept low (less than 10 MOhm in most recordings of BLA principal neurons) by using patch pipettes with a larger tip (2 μm in outer diameter). For intercalated neurons, EPSCs were recorded from 1-2 cells in the two most caudal slices per hemisphere, where clusters of intercalated neurons were readily identifiable with the IR-DIC optics. Collecting and analyzing data from large numbers of mice and recorded neurons, it was possible to decrease the variability further in *ex vivo* electrophysiological experiments. After completion of electrophysiological recordings, slices were fixed and microscopic photographs were taken for all mice used in this study. Using fluorescent microscopy, GFP signal in the mPFC was reexamined to verify the location of AAV injection sites and the extent of

ChR2 expression. When the target (IL/mPFC) for AAV injections was missed, recording data from these particular mice were excluded from the analysis.

Supplemental Text

Evidence that photostimulation-induced EPSCs in amygdala were monosynaptic in origin

Application of TTX (1 μM) completely blocked EPSCs recorded in mPFC-BLA pathway (Figures 1H and S3A), indicating that optogenetically-evoked EPSCs require action potential firing in axons from the mPFC. This also suggests that ChR2-mediated depolarization by photostimulation alone is insufficient to induce neurotransmitter release from nerve terminals. We reasoned that inhibition of voltage-gated K^+ channels by 4-aminopyridine (4-AP) may induce additional depolarization at terminals so that ChR2-mediated depolarization may now be sufficient to trigger glutamate release even in the presence of TTX, resulting in EPSCs in postsynaptic BLA principal neurons (Petreanu et al., 2009). Notably, the rescue of TTX-blocked EPSCs by 4-AP may be observed only if ChR2-expressing mPFC fibers project monosynaptically to postsynaptic BLA neurons (Figure S3B). This is because only mPFC fibers terminating in the BLA, but not BLA neurons themselves express ChR2. Thus, the application of 4-AP would not rescue any TTX-blocked polysynaptic components, possibly arising from local connection and, therefore, requiring AP firing by BLA neurons in the local network. Consistent with monosynaptic nature of the mPFC-BLA projections, 4-AP (1 mM) rescued EPSC partially in the presence of TTX ($p < 0.001$ versus TTX only, Figures S3A and S3C).

Partial recovery of photostimulation-evoked EPSCs by 4-AP was also described in previous reports (Petreanu et al., 2009). The incompleteness of recovery could,

probably, be explained by the fact that depolarization by ChR2 activation and inhibition of voltage-gated K^+ channels may not be as effective in inducing presynaptic Ca^{2+} influx and triggering glutamate release at axon terminals as ChR2-induced action potential firing in the absence of TTX. Alternatively, the mPFC-BLA EPSCs recorded under control conditions may be mixed, containing both monosynaptic and polysynaptic components, whereas 4-AP was only rescuing monosynaptic responses. To test for the latter possibility, we compared decay time constants between EPSCs recorded under control conditions and EPSCs recorded in the presence of TTX + 4-AP. If control EPSCs contained significant polysynaptic contributions, EPSCs under control conditions would have slower decay kinetics (Figure 4I) compared to purely monosynaptic EPSCs recorded in the presence of TTX + 4-AP. However, we did not observe a significant difference in decay time constants between these two conditions (Figure S3C; $p = 0.29$, paired t test), arguing against a possibility of polysynaptic contributions. We also confirmed the validity of this approach by showing that 4-AP did not rescue optogenetically-activated disynaptic IPSCs in the mPFC-BLA/IN-BLA/PN pathway in the presence of TTX (Figure S3D). Thus, 4-AP failed to rescue TTX-blocked synaptic responses, requiring AP firing in axons, which do not express ChR2 (interneurons in the BLA). Moreover, electrical stimulation-evoked monosynaptic EPSCs in projections form the auditory cortex to the BLA were not rescued by 4-AP in the presence of TTX (Figure S3E).

The analysis of synaptic latencies indicated that intercalated neurons also receive monosynaptic projections from the mPFC (Figure 7B). To confirm this, we performed similar experiments in the mPFC-ITC pathway using 4-AP. TTX application

blocked EPSCs in intercalated cells evoked by photostimulation of ChR2-expressing mPFC fibers (Figure S3G). As in the experiments focusing on the mPFC-BLA pathway, the application of 4-AP rescued TTX-blocked EPSCs in intercalated neurons, confirming monosynaptic nature of EPSCs in intercalated cells induced by photostimulation of mPFC fibers. We also confirmed monosynaptic nature of connections between the mPFC fibers and local GABAergic interneurons in the BLA (BLA/IN) by showing that the application of 4-AP similarly rescued TTX-blocked, optogenetically-induced EPSCs recorded in BLA/IN (Figure S3F). These findings support the notion that EPSCs in the mPFC-BLA/IN or mPFC-ITC projections, recorded in our study, were monosynaptic in origin.